

RXTE OBSERVATIONS OF LMC X-1

P.C. Schmidtke, A.L. Ponder, and A.P. Cowley

Department of Physics & Astronomy, Arizona State University, Tempe, AZ, 85287-1504

ABSTRACT

The luminous X-ray binary and black-hole candidate LMC X-1 has been observed with the Rossi X-ray Timing Explorer (*RXTE*) to search for quasi-periodic oscillations (QPO), previously reported in its high state. The source was observed monthly in a series of nine observations. Analysis of the temporal variations shows no evidence for QPO or other periodic changes, but correlations between the high-energy light curve and hardness of the spectrum are described. Spectral fits with two-component models demonstrate that the hardness variations come from changes in the intensity of the high-energy power-law tail.

Subject headings: X-rays: stars – binaries: close – stars: oscillations – Magellanic Clouds

1. INTRODUCTION

LMC X-1 is one of four extremely luminous ($> 10^{38}$ ergs s $^{-1}$) X-ray binaries in the Large Magellanic Cloud. The source has long been known to show a rather soft X-ray spectrum ($kT \sim 2.7$ keV; Markert & Clark 1975) and irregular X-ray variability by at least a factor of three (Griffiths & Seward 1977, Johnston, Bradt, & Doxsey 1979). However, its optical identification was uncertain for many years. The source lies within the bright emission nebula N159 (Henize 1956) containing many early-type stars (see finding chart of region in Cowley, Crampton, & Hutchings 1978). Based on the rather uncertain X-ray position, it was originally thought that the B5 supergiant R148 ($V \sim 12.5$) was the optical counterpart, although the peculiar O7 III star (Star #32 of Cowley et al.) 6'' away could not be ruled out. Recent analysis of *ROSAT* High-Resolution Imager data has confirmed that Star #32 ($V \sim 14.8$) is the most probable identification (Cowley et al. 1995). Spectroscopic studies of this star reveal an orbital period near 4 days and a probable mass for the compact star of $M_X \sim 4M_\odot$ (Hutchings, Crampton, & Cowley 1983, Hutchings et al. 1987), making it a strong black-hole candidate.

Because LMC X-1 is so luminous, its X-ray properties were studied even with the earliest X-ray detectors. White & Marshall (1984) discussed the complex character of its X-ray spectrum, showing that it could not be described by a simple model because of the high-energy excess above 3 keV. Thus a two-component model with a soft thermal spectrum and plus a hard high-energy tail was needed. They pointed out the similarity in spectral properties of LMC X-1 to another black-hole candidate, LMC X-3, and they were the first to recognize that an unusually soft X-ray spectrum may be a reliable signature of a black-hole candidate.

Using *Ginga* data, Ebisawa, Mitsuda, & Inoue (1989) also found a two-component model was needed to fit the spectrum: an ultrasoft blackbody ($kT \sim 0.8$ keV) and a hard power law (photon index ~ 2.5). Later, Schlegel et al. (1994a, 1994b) modeled the spectrum, based on Broad Band X-ray Telescope (BBXRT) data, finding results similar to those of Ebisawa et al.

Ebisawa et al. undertook a timing analysis of their *Ginga* data and found quasi-periodic oscillations (QPO) with a peak frequency of 0.0751 Hz in one of the observations. They concluded that the QPO came from the hard-tail component, which was unusually bright at the time in comparison to the thermal component. QPO were not found in the BBXRT data (Schlegel et al.), confirming the transient nature of these aperiodic signals. Since the presence of QPO might be related to the spectral state of the system, we undertook a series of observations with Rossi X-ray Timing Explorer (*RXTE*) over a period of nine months to search for QPO and to further define their origin.

2. OBSERVATIONS AND DATA ANALYSIS

A series of nine observations were made between 1996 February and 1996 October. Table 1 lists the details of the observational data, in reverse time order, following the numbering system of the *RXTE* Science Data Center. Only data from the Proportional Counter Array (PCA) were analyzed due to the very low net count rate for events with energies >16 keV. Each observation was broken into two or three segments due to Earth occultations or passages through the South Atlantic Anomaly. In 1996 March, two proportional counter units (PCU) were found to be discharging, making it necessary to shut them down periodically. The result was that some observations were made with only three of the five PCU operating (observations #4, #6, and #7), as noted in Table 1. Observation #3 experienced a shutdown of two PCU during the second half of the exposure, so it was necessary to analyze this observation in two parts (#3A and #3B).

2.1. Light Curves and Hardness Ratios

Background-subtracted light curves, using 16-s time bins, were derived for the 2–5.9 keV and 5.9–15.9 keV energy ranges. The spectral hardness within each bin was found by calculating the ratio of counts, $HR = (5.9\text{--}15.9 \text{ keV})/(2\text{--}5.9 \text{ keV})$. Typical values for the hardness ratio are $\sim 0.1\text{--}0.2$; mean values for each observation are listed in Table 1. The light and HR curves for observations #2, #3B and #4 are shown in Fig. 1. The selected observations span a wide range of source intensity and hardness. In observation #3B (‘average’ count rate; lowest HR) LMC X-1 was in a quiescent mode with minimal flickering, while in both #2 (second highest count rate; highest HR) and #4 (lowest count rate; ‘average’ HR) the source varied rapidly on a time scale of minutes. Examination of all of the observations reveals no dependence of the source’s flickering characteristics on either the count rate or hardness. However, for each observation the plot of hardness ratio is similar to that of the high-energy count rate, implying the ratio is driven primarily by the number of 5.9–15.9 keV counts. *Ginga* data for the black hole candidate GX 339–4 in its very high state (Miyamoto et al. 1991) show the same behavior (see their Fig. 2). While in this very high state, the source is 2–3 \times more intense and shows significantly enhanced variability (on timescales of minutes) compared to when it is in a (relatively quiescent) high state (Makishima et al. 1986). Although the *RXTE* observations also show various degrees of short-term variability, there is no clear indication that LMC X-1 enters a very high spectral state.

To test the dependence of HR on the source count rate, we used data from all observations to construct the hardness-intensity diagrams shown in Fig. 2. The plot of HR versus low-energy count rate has no significant relationship between the parameters. However, the plot of HR versus 5.9–15.9 keV count rate exhibits a very strong correlation which is also present in each of the individual observations. This dependence confirms the trend inferred from examination of the simple light and hardness-ratio curves.

We examined the data for time lags between high and low-energy photons by calculating the cross-correlation of the two light curves. A small positive lag, in the sense that high-energy photons tend to arrive after their low-energy counterparts, was found for all observations. However, the mean lag time in each case was comparable to the 0.025-s step used in the calculations, so that the results are not conclusive.

2.2. Power Density Spectra and Quasi-periodic Oscillations

To further investigate the temporal variations, power density spectra (PDS) were constructed using the background-subtracted data, rebinned at 0.125-s resolution. Within an observation, the Fourier transformation was calculated for each 512-s data segment (4096 points), covering the frequency range 0.002–4 Hz. Typically, each PDS represents the average of ~ 11 individual transforms. Two sets of PDS were made, one covering the entire PCA energy range (2–60 keV) and the other restricted to primarily those photons in the hard spectral tail (5.9–15.9 keV). No significant differences between these were found. In Fig. 3 we present the power density spectrum (5.9–15.9 keV) for observation #7. The power density increases at low frequency (i.e., red noise) and can be modeled in terms of a power law plus a constant (i.e., $\text{power} = \nu^{-\alpha} + C$, where α is the power index). Fitted values of the power index, for both the 5.9–15.9 keV and 2–60 keV PDS, are listed in Table 2. The average indices are $\alpha = 1.06$ and 0.87 for the restricted and full energy ranges, respectively. There is no significant dependence of the modeled power index with either the hardness ratio or the source count rate. For comparison, Ebisawa et al. (1989) measured an index of 0.81 in a *Ginga* observation taken when LMC X-1 was in an X-ray bright state.

If present, quasi-periodic oscillations would appear as a broad peak in the PDS. None of our observations shows this signature, although Ebisawa et al. found strong QPO near 0.0751 Hz in some of the *Ginga* data, with weaker QPO around 0.142 Hz. (Most likely, this other peak is the second harmonic.) Upper limits for the amplitude of QPO signals in the *RXTE* observations were found by calculating the percent r.m.s. variation of the average excess power (after subtracting the fitted model) between 0.05 and 0.10 Hz. Typical 3σ limits are $\sim 0.8\%$ for the 2–60 keV PDS, as listed in Table 2. For comparison, the amplitudes of the primary and secondary *Ginga* QPO peaks were 2.9% r.m.s. and 1.8% r.m.s., respectively. Hence, the power found in the *Ginga* QPO was much larger than the upper limits placed on the *RXTE* data. Clearly, the appearance of QPO in LMC X-1 is a transient phenomenon, as further documented by the lack measurable QPO in BBXRT observations of this source (Schlegel et al. 1994a, 1994b).

2.3. Spectral Fits

The X-ray energy spectrum of LMC X-1 was separately fit by two multi-component models over the energy range 3.6–15.9 keV. The soft thermal component was represented by both a blackbody and by a multicolor disk model (Mitsuda et al. 1984; Makishima et al. 1986), while the high-energy excess was always accounted for using a simple power law. Within limitations imposed by an uncertain background subtraction at low energies

in the *RXTE* data, both combinations yield acceptable fits. The intervening hydrogen absorption was fixed at $N_H = 0.6 \times 10^{22} \text{ cm}^{-2}$ in all cases, since the derivation of N_H as a free parameter is very sensitive to errors in background subtraction. Mean values for the fitted parameters, which are similar to those of Ebisawa et al. (1989) and Schlegel et al. (1994a), are summarized in Table 3. Since the hardness ratio depends on source intensity, further modeling was performed on data selected by PCA count rate count (i.e., 130–140 cts s⁻¹, 140–150 cts s⁻¹, etc.). The results of this fitting for the blackbody plus power-law model are shown in Fig. 4. Within each observation, we find a trend for an increasing ‘scale’ of the power law (i.e., comparable to intensity provided the photon index is constant) with increasing source count rate (3.6–15.9 keV). The remaining parameters are nearly constant within a given observation, although a slight increase in temperature of the thermal component may be present at higher count rates. We note that the fitted parameters are highly coupled. If the temperature of the soft component were held constant, then the dependence of the power-law scale on count rate would become even more pronounced.

2.4. Long-term and Phase-related Variations

The All Sky Monitor (ASM) aboard *RXTE* provides nearly continuous monitoring of the entire sky, producing long-term light curves for bright, persistent X-ray sources as well as discovering new transient sources. We have examined the LMC X-1 data in this public archive. They compare well with the mean count rates for our pointed observations, as presented in this paper. Overall, the source varied by about a factor of two through the nine months during which our observations were taken. Analysis of ~ 3500 ASM data points taken over 76 weeks of observing does not reveal any significant periods in the range 0.5–20 days, including at the optically determined orbital period of 4.22 days. This result has been confirmed by scientists on the instrument team (Levine 1997).

In addition to searching for periods in the ASM observations, we have folded our *RXTE* data on the 4.22-day orbital period. The phase coverage is poor because the observations were only obtained at nine discrete times. As it turned out, no observations were obtained between spectroscopic phases 0.9 to 1.3, leaving a large gap in the phase plots. From the folded data there is no clear indication of any trends related to the orbital period either in the count rate or the hardness ratio. Additional data obtained at more closely spaced intervals are needed to determine if any small orbital modulation or other signature is present in the X-ray data.

3. SUMMARY

We obtained a series of *RXTE* observations of the black-hole candidate LMC X-1 to search for quasi-periodic oscillations and examine their behavior with source intensity. No QPO were detected, although Ebisawa et al. had detected them in LMC X-1 when the source was in a bright state. Comparison of the source intensity during the *RXTE* and *Ginga* observations suggests that LMC X-1 never became as bright during our *RXTE* observations as when QPO were found in *Ginga* data. However, because of the uncertainty of the background subtraction with the *RXTE* data, it is difficult to compare these data sets. In addition, no other periodic behavior was found, either on the orbital period or any other in the range of 0.5-20 days.

Fits of the X-ray spectral energy distribution require a two-component model, and the values derived are similar to those found by previous workers. A strong correlation was detected between the hardness ratio and the high-energy count rate, indicating that changes in the X-ray spectrum of LMC X-1 come from the high-energy tail.

We wish to thank the staff at the *RXTE* Guest Observer Facility. We also acknowledge support from NASA.

Table 1: Summary of *RXTE* Observations

Obs. #	Date yy/mm/dd	Start Time UT	Exp. Time s	Count Rate ^a cnts s ⁻¹	Hardness Ratio ^b
1	96/10/04	12:35:12	4912	155.6±0.3	0.15±0.03
2	96/09/06	21:45:52	6880	162.2±0.3	0.23±0.05
3B	96/08/01	22:12:32	2880	151.0±0.3 ^c	0.10±0.02
3A	96/08/01	21:02:56	3664	160.6±0.3	0.13±0.02
4	96/07/05	01:59:44	5328	135.2±0.4 ^c	0.15±0.04
5	96/06/09	20:22:24	6800	148.8±0.3	0.14±0.03
6	96/05/18	07:32:48	6656	159.2±0.4 ^c	0.15±0.03
7	96/04/18	06:45:52	5840	168.2±0.4 ^c	0.15±0.03
8	96/03/08	05:39:12	4976	148.1±0.3	0.22±0.06
9	96/02/10	05:31:12	9504	155.1±0.3	0.18±0.03

^aBackground-subtracted PCA count rate (2–60 keV)

^bHardness ratio = (5.9–15.9 keV count rate)/(2–5.9 keV count rate)

^cCorrected to account for shutdown of two PCU

Table 2: Power Density Spectrum Parameters

Obs. #	Power Index ^a 5.9–15.9 keV	Power Index ^a 2–60 keV	QPO Power ^b 2–60 keV
1	0.83 ± 0.07	0.63 ± 0.05	< 0.4%
2	0.99 ± 0.02	0.88 ± 0.01	< 0.2%
3B	1.09 ± 0.09	1.01 ± 0.04	< 0.8%
3A	1.17 ± 0.12	1.17 ± 0.06	< 1.0%
4	0.78 ± 0.03	0.64 ± 0.01	< 1.8%
5	0.94 ± 0.09	0.93 ± 0.05	< 0.5%
6	1.44 ± 0.07	1.09 ± 0.03	< 0.6%
7	0.98 ± 0.03	1.02 ± 0.01	< 1.6%
8	1.49 ± 0.03	0.85 ± 0.01	< 0.9%
9	0.86 ± 0.04	0.52 ± 0.03	< 0.2%

^aModeled using $\nu^{-\alpha} + C$, where α is the power index

^b 3σ upper limit for r.m.s. variation of average excess power between 0.05–0.10 Hz

Table 3: Mean Spectral Fitting Parameters

<u>Model: Blackbody plus power law</u>	
Radius of blackbody ^a	40 km
Temperature of blackbody	0.88 keV
Photon index of power law	2.44
Scale of power law	2.08×10^{-4} photons keV ⁻¹ cm ⁻² s ⁻¹ at 10 keV
N_H	0.6×10^{22} atoms cm ⁻² (fixed)
<u>Model: Multicolor disk plus power law</u>	
Projected size of inner disk radius ^{a,b}	22 km
Temperature of inner disk radius	1.17 keV
Photon index of power law	1.45
Scale of power law	1.42×10^{-4} photons keV ⁻¹ cm ⁻² s ⁻¹ at 10 keV
N_H	0.6×10^{22} atoms cm ⁻² (fixed)

^aFor an assumed distance of 50 kpc

^b $R_{in} \cos^{1/2} \theta$

REFERENCES

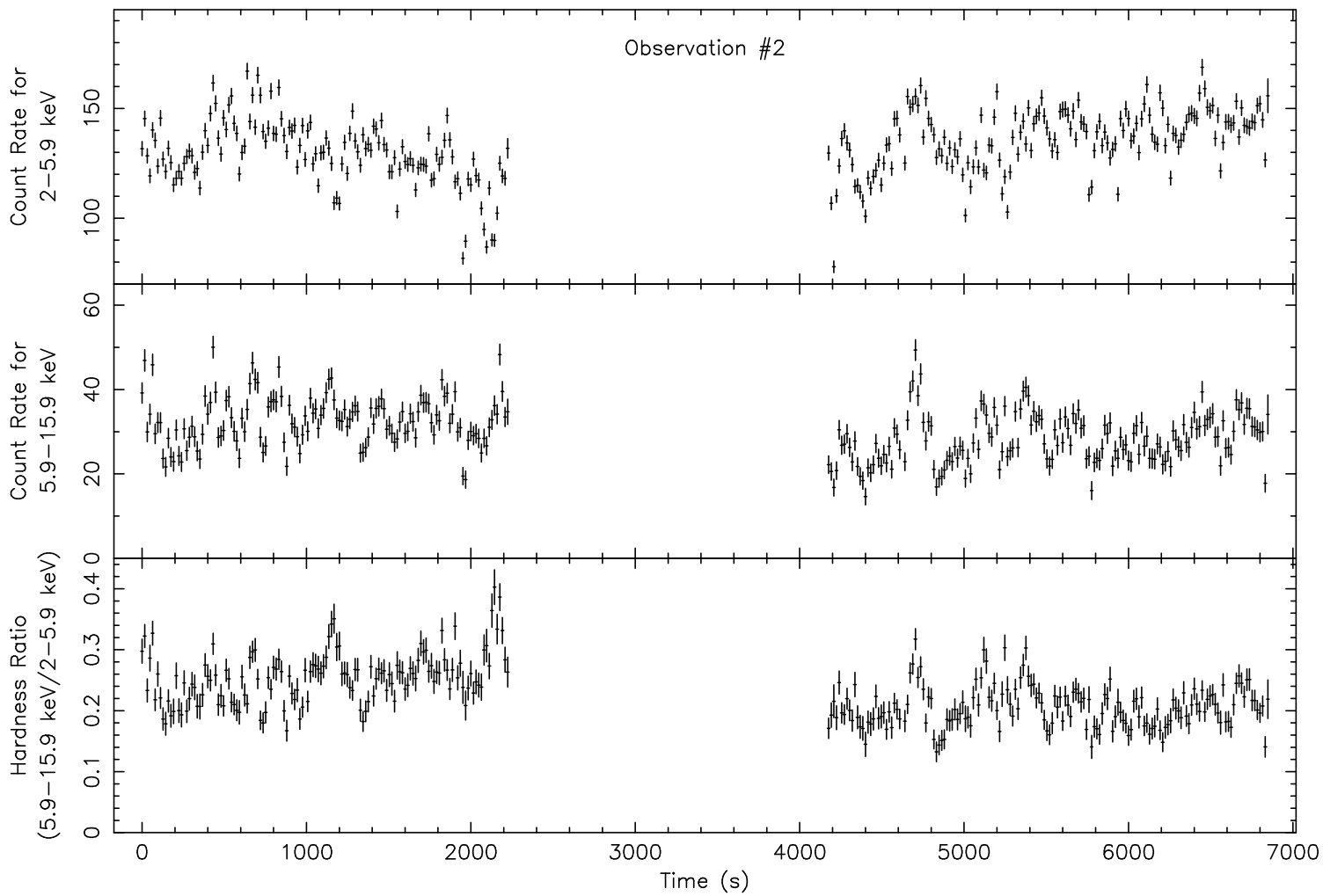
- Cowley, A.P., Schmidtke, P.C., Anderson, A.L., & McGrath, T.K. 1995, *PASP*, 107, 145
- Cowley, A.P., Crampton, D., & Hutchings, J.B. 1978, *AJ*, 83, 1619
- Ebisawa, K., Mitsuda, K., & Inoue, H. 1989, *PASJ*, 41, 519
- Griffiths, R.E. & Seward, F.D 1977, *MNRAS*, 180, 75P
- Henize, K.G. 1956, *ApJS*, 2, 315
- Hutchings, J.B., Crampton, D., & Cowley, A.P. 1983, *ApJ*, 275, L43
- Hutchings, J.B., Crampton, D., Cowley, A.P., Bianchi, L., & Thompson, I.B. 1987, *AJ*, 94, 340
- Johnston, M.D., Bradt, H.V., & Doxsey, R.E. 1979, *ApJ*, 233, 514
- Levine, A. 1997, private communication
- Makishima, K., et al. 1986, *ApJ*, 308, 635
- Markert, T.H. & Clark, G.W. 1975, *ApJ*, 196, L55
- Mitsuda, K., et al. 1984, *PASJ*, 36, 741
- Miyamoto, S., Kimura, K., Kitamoto, S., Dotani, T., & Ebisawa, K. 1991, *ApJ*, 383, 784
- Schlegel, E.M. et al. 1994a, *ApJ*, 422, 243
- Schlegel, E.M. et al. 1994b, in “The Evolution of X-ray Binaries”, eds. S.S. Holt & C.S. Day, *AIP Conf. Proc.*, 308, 119
- White, N.E. & Marshall, F.E. 1984, *ApJ*, 281, 354

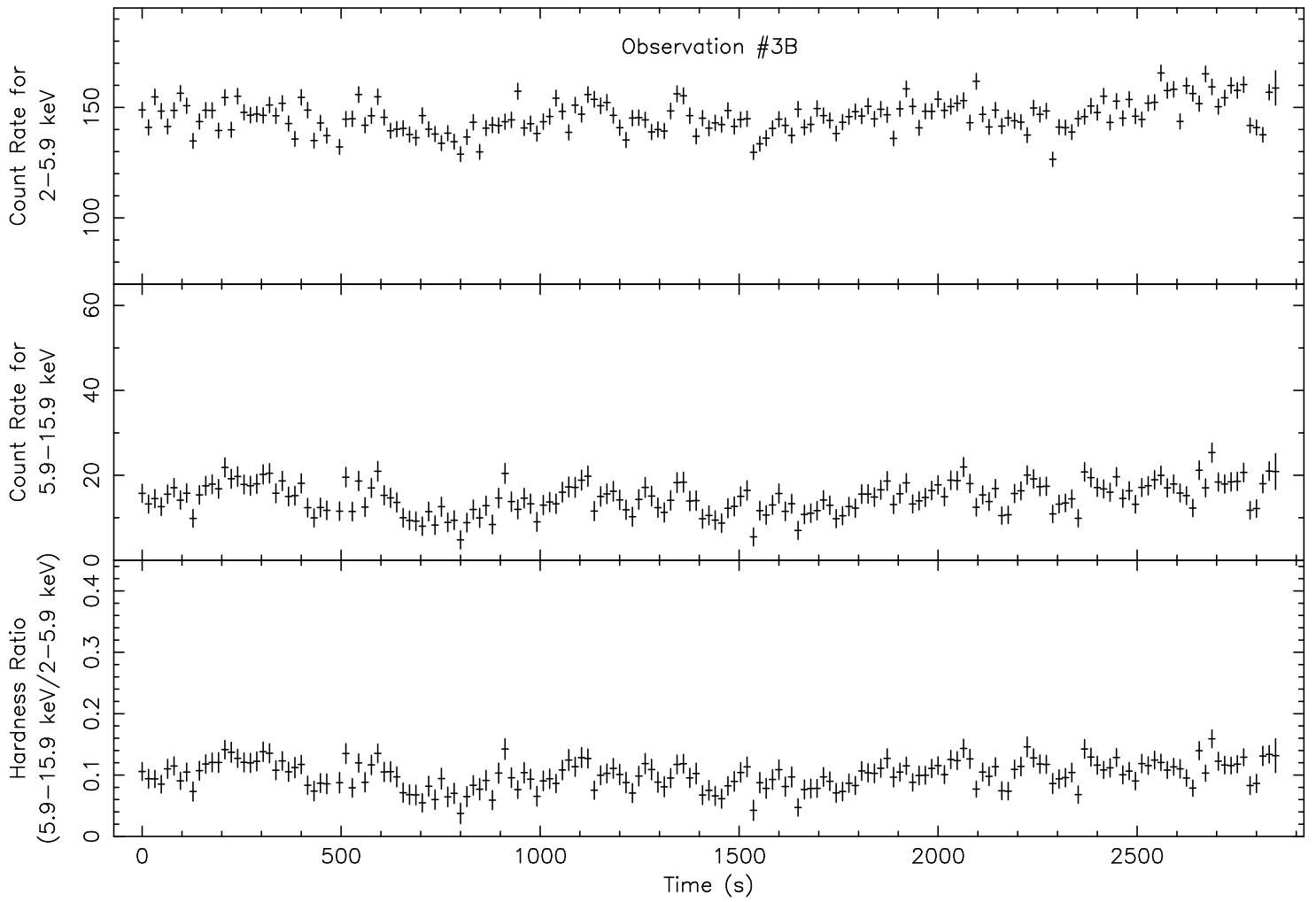
Fig. 1.— *RXTE* data for observations #2, #3B, and #4 of LMC X-1; the top and middle panels are X-ray light curves for the energy ranges 2–5.9 keV and 5.9–15.9 keV, respectively. The bottom panels show the hardness ratio (5.9–15.9 keV/2–5.9 keV). Note the similarity of the high-energy light curves and the hardness ratio. The other observations have similar characteristics. The short-term variability does not appear to depend on either source intensity or hardness.

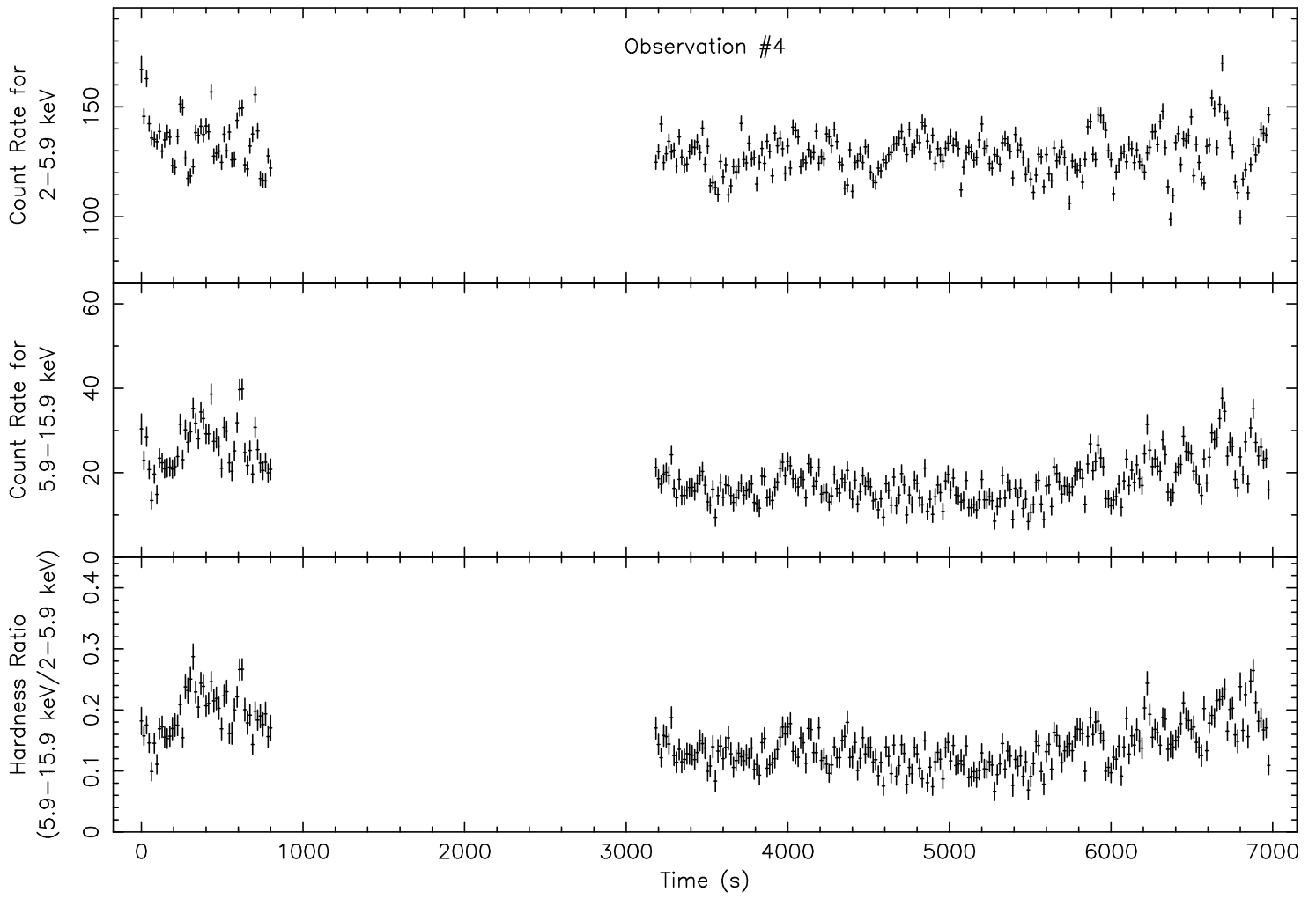
Fig. 2.— Hardness ratio versus count rate in the 2–5.9 keV and 5.9–15.9 keV energy ranges for all *RXTE* observations of LMC X-1. Although there is no relationship between hardness and the low-energy counts, the ratio is strongly correlated with the high-energy count rate. This correlation is present in each observation.

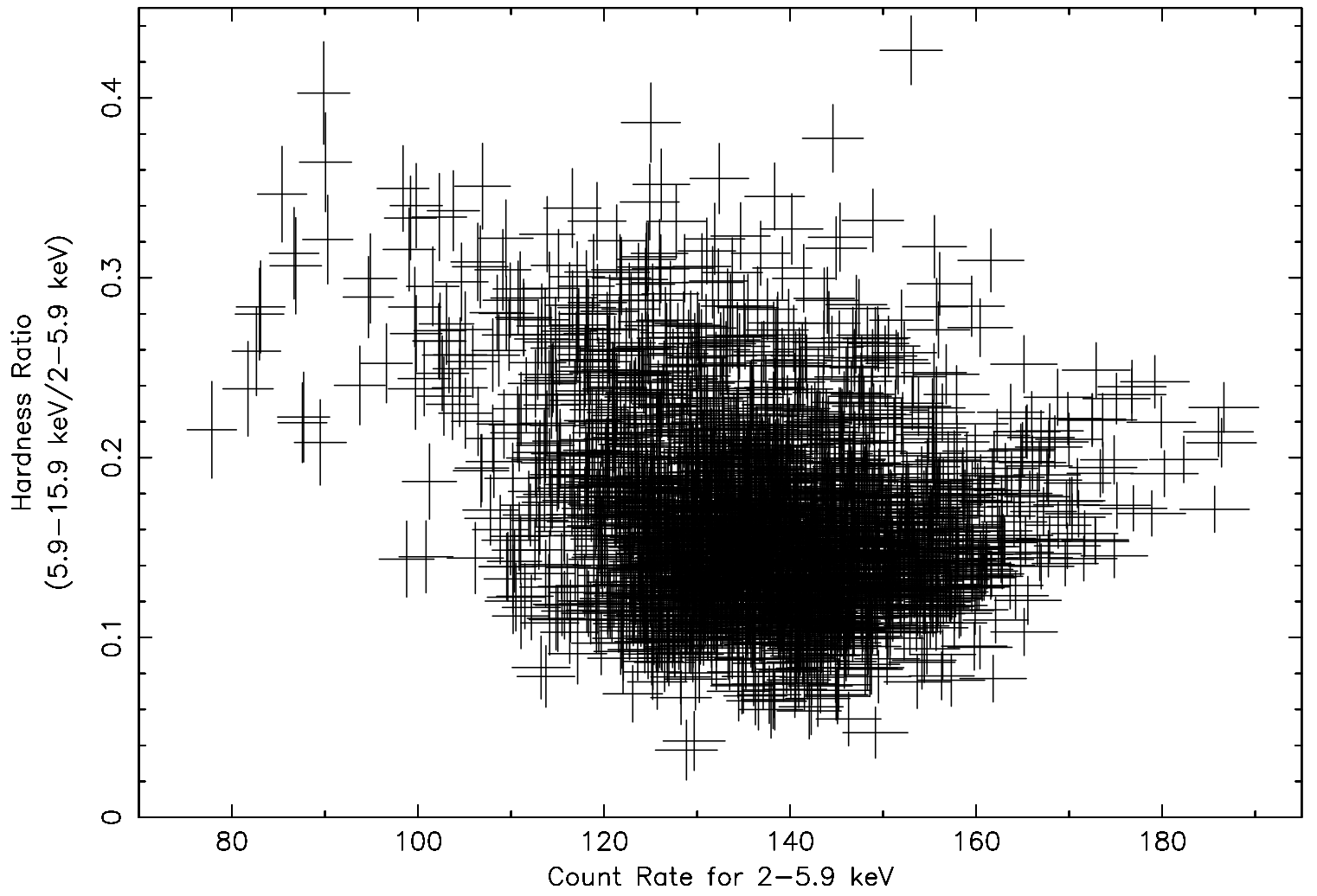
Fig. 3.— Power density spectrum of LMC X-1 for *RXTE* observation #7 using 0.125-s bins over the energy range 5.9–15.9 keV. The best-fit curve is a power law plus a constant (i.e., power = $\nu^{-\alpha} + C$). There is no evidence for QPO in this or any of the other PDS within the frequency range 0.002–4 Hz.

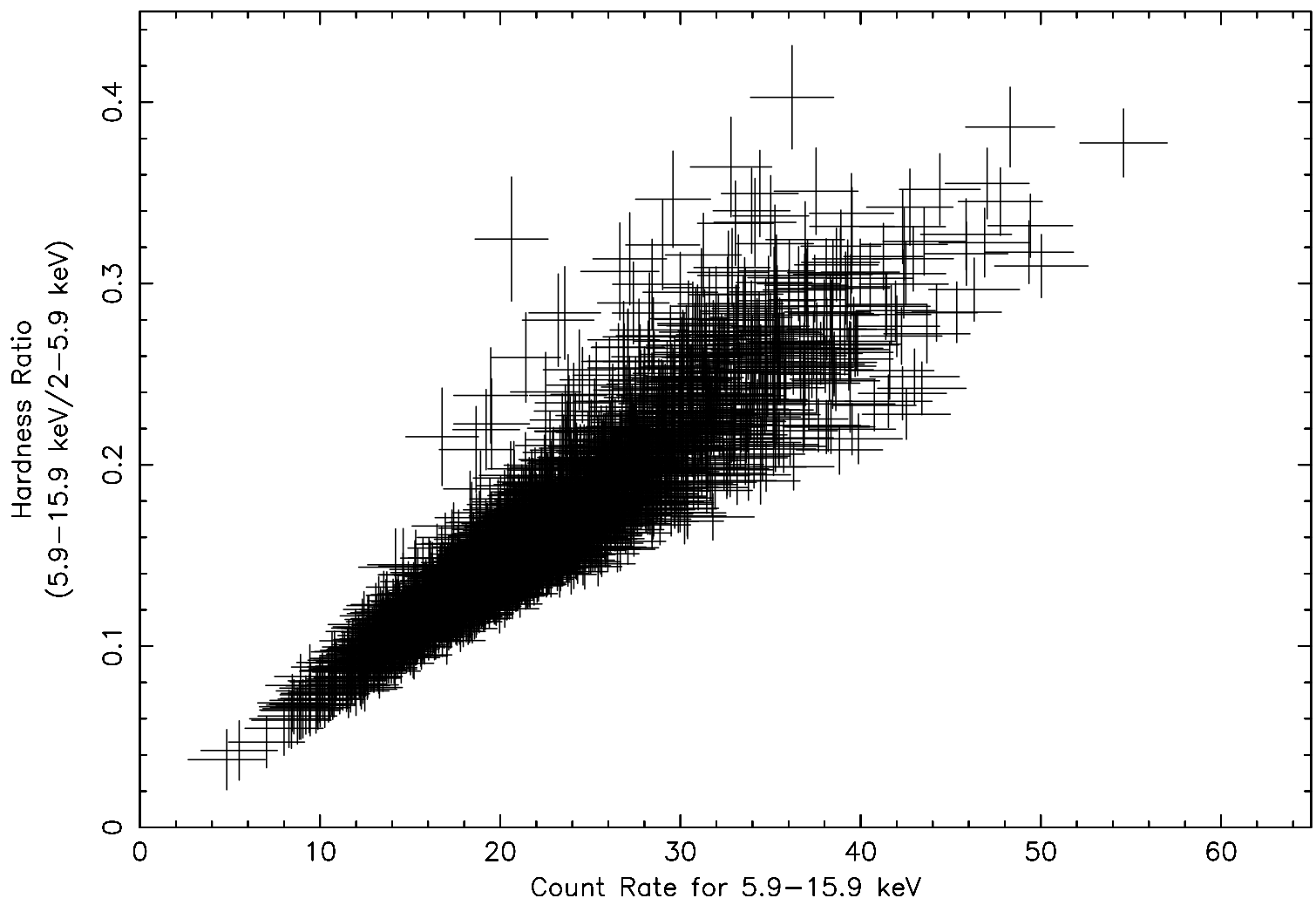
Fig. 4.— Parameters of the blackbody plus power-law model versus mean count rate (3.6–15.9 keV), with different observations of LMC X-1 indicated by separate symbols. The fitting was done over the 3.6–15.9 keV energy range, on subsets of data selected by PCA count rate.

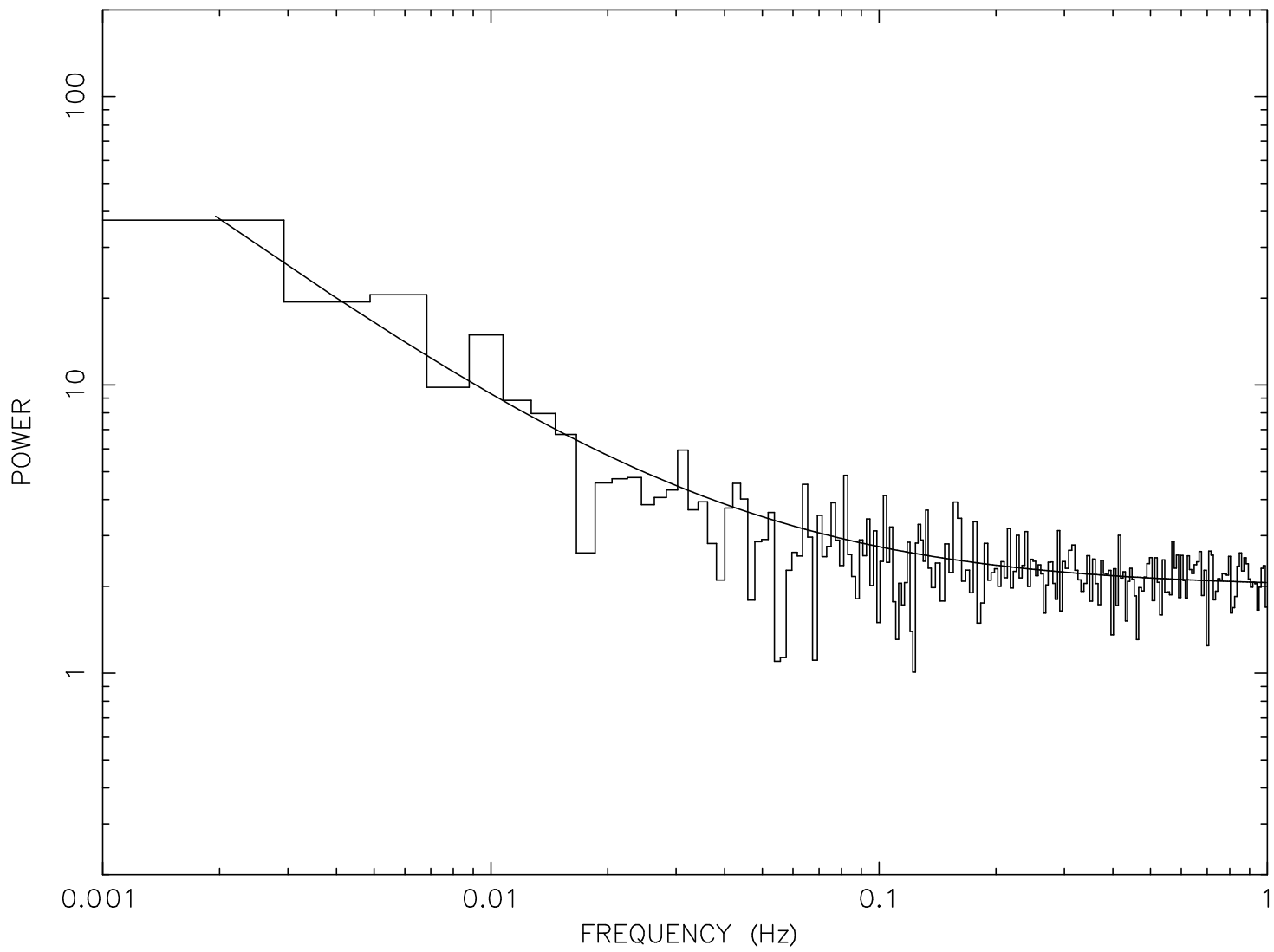




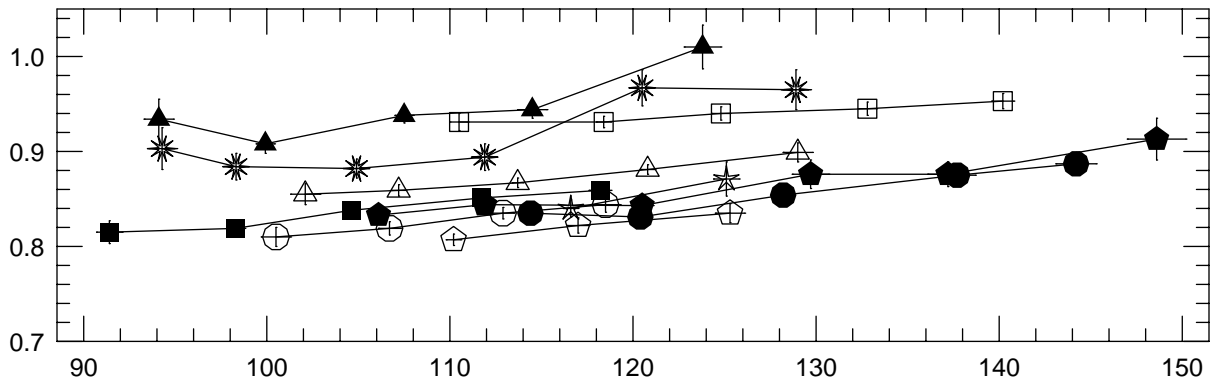




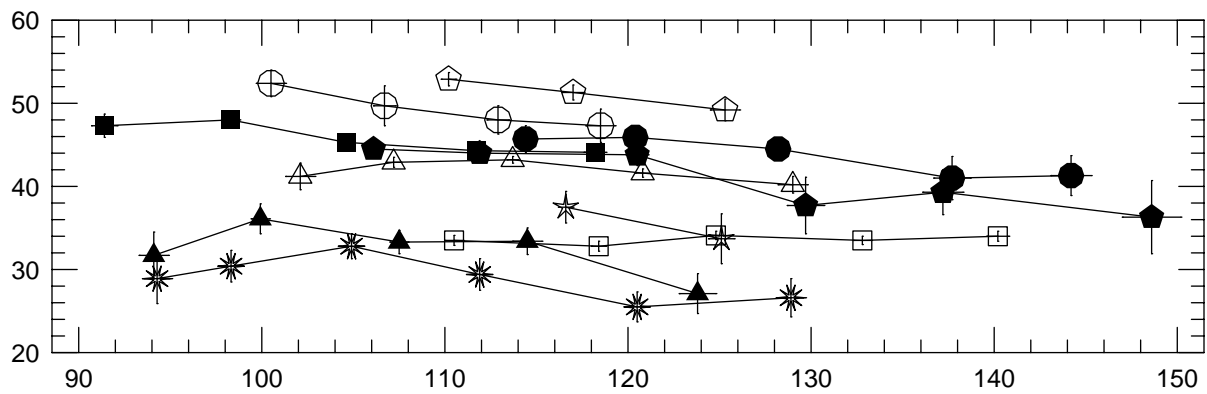




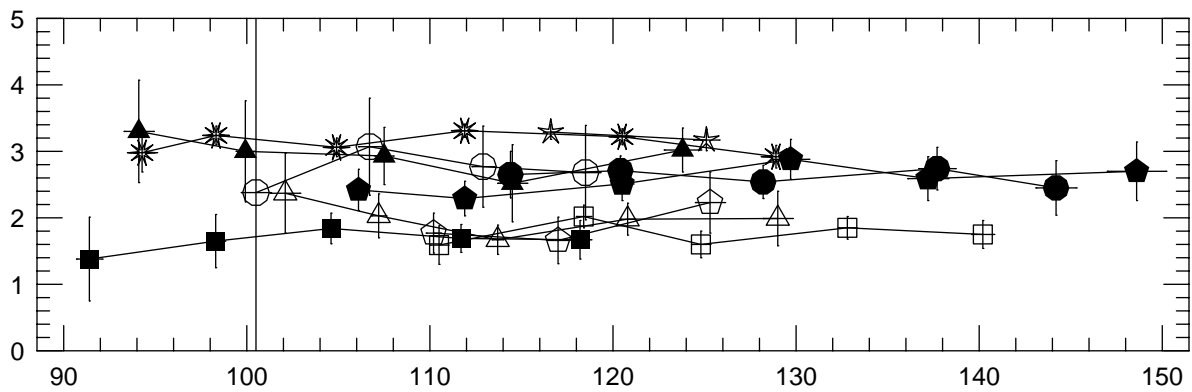
Temperature (keV)



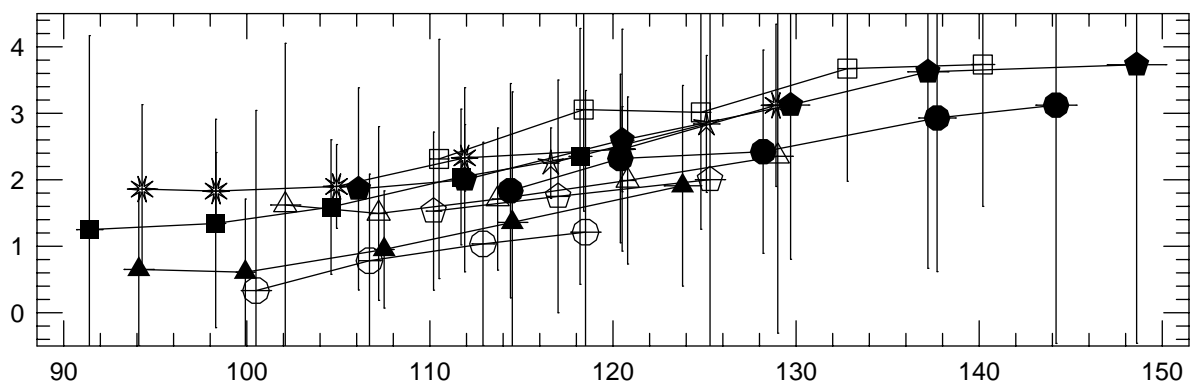
Radius (km)



Photon Index



Scale at 10 keV
($\times 10^{-4}$ photons/keV/cm²/s)



Count Rate (cnts/s)